GEOPHYSICAL RESEARCH LETTERS, VOL. 24, NO.8, PAGES 995-998, APRIL 15, 1997

Remote determination of auroral energy characteristics during substorm activity

G. A. Germany[1], G. K. Parks[2], M. Brittnacher[2], J. Cumnock[3], D. Lummerzheim[4], J. F. Spann[5], L. Chen[2], P. G. Richards[6], and F. J. Rich[7]

Abstract. Ultraviolet auroral images from the Ultraviolet Imager (UVI) onboard the POLAR satellite can be used as quantitative remote diagnostics of the auroral regions, yielding estimates of incident energy characteristics, compositional changes, and other higher order data products. Here incident energy estimates derived from UVI are compared with *in situ* measurements of the same parameters from an overflight by the DMSP F12 satellite coincident with the UVI image times during substorm activity occurring on May 19, 1996. This event was simultaneously observed by WIND, GEOTAIL, INTERBALL, DMSP and NOAA spacecraft as well as by POLAR.

Introduction

Images of the auroral regions from space have proven invaluable in determining auroral morphology and correlating substorm onset time with extended groundbased and spacebased observations such as those available within the International Solar Terrestrial Physics (ISTP) program. With the advent of new imaging technologies and increased modeling capabilities the emphasis has shifted toward using global auroral images as quantitative remote diagnostics of the incident energy flow into the auroral regions. In particular, the determination of incident energy flux and average energy is fundamental to the characterization of the auroral processes.

The Ultraviolet Imager (UVI) [*Torr et al.*, 1995] is one of three imagers aboard the Global Geospace POLAR spacecraft. The POLAR apogee of 9 Earth radii, combined with its despun observing platform, provides an unprecedented opportunity to view the entire northern auroral region for extended periods of several hours. By imaging in the far ultraviolet, UVI is capable of viewing both nightside and sunlit auroral features. The advanced filter technology employed in the Ultraviolet Imager allows separation of far ultraviolet (FUV) emission features within the UVI field of view. These emission features can be used to estimate the incident auroral characteristics on a per pixel basis.

[1]Center for Space Plasma and Aeronomic Research, University of Alabama in Huntsville, Huntsville.
[2]Geophysics Department, University of Washington, Seattle.
[3]Space Physics Research Laboratory, University of Michigan, Ann Arbor.
[4]Geophysical Institute, University of Alaska, Fairbanks.
[5]NASA Marshall Space Flight Center, Huntsville, AL.
[6]Computer Science Department, University of Alabama in Huntsville, AL.
[7]Geophysics Dir., USAF Phillips Laboratory, Hanscom AFB, MA.

Paper number 97GL00864.
0094-8534/97/97GL-00864$05.00

In this study UVI images taken during substorm activity on May 19, 1996 are used to determine energy maps of the incident auroral energy characteristics. These maps are then compared with *in situ* measurements of the same parameters by the DMSP F12 spacecraft.

Technique

The technique for using FUV emissions as remote diagnostics has been discussed elsewhere [*Strickland et al.*, 1983; *Germany et. al.*, 1994a,b; 1990; *Lummerzheim et al.*, 1991] and will only be summarized here. The principal emissions within the UVI spectral bandpass (125.0 - 200.0 nm) are atomic oxygen emissions and molecular N_2 Lyman-Birge-Hopfield (LBH) emissions. Atomic nitrogen lines also appear at 149.3 and 174.6 nm. The LBH emissions are electric dipole forbidden and the only prominent excitation mechanism is electron impact excitation. Thus, in the absence of dayside photoelectrons, observed LBH intensities are direct diagnostics of the incident auroral flux. The O_2 Schumann-Runge absorption continuum peaks within the UVI bandpass, decreasing with longer wavelength. FUV auroral emissions viewed from space in the spectral region of strong O_2 absorption will exhibit losses, provided the incident auroral energy is high enough to reach the lower altitudes where O_2 density is greatest. The observed emissions vary strongly (inversely) with increasing depth of penetration of the incident auroral electrons and hence with increasing energy.

The N_2 LBH emissions can be divided into two regions: one at shorter wavelengths with significant losses due to O_2 absorption (denoted LBHs and extending roughly from 140 to 160 nm) and longer wavelength emissions with less loss (LBHl, 160 to 180 nm). Modeling of expected emissions can be used to estimate incident energy flux from LBHl intensities and the average energy from the ratio of either OI 135.6 or LBHs to LBHl. The 135.6 nm emission is dependent on changes in the atomic oxygen density and can therefore exhibit significant variability. The LBH emissions also exhibit variability with changes in N_2 density, though these changes are not as great as those for the OI 135.6 emission. However, since the emissions in the LBHs and LBHl filter passbands originate from the same species, their ratio is nearly independent of compositional changes with season or over a solar cycle [*Germany et al.*, 1990]. The following discussion is therefore limited to the analysis of the LBHs/LBHl ratio.

In the ideal case, UVI energy analysis would be performed with two LBH bands - one at the wavelength of peak absorption near 140 nm and the other at a longer wavelength where O_2 absorption is negligible, i.e. greater than 170 nm. The longer wavelength emission would be essentially independent of average energy and solely dependent on

energy flux. This is the case modeled previously by *Germany et. al.* [1994a,b; 1990]. In practice, the UVI LBH filters must necessarily include multiple LBH bands and therefore contain a range of loss factors. Thus the LBHl emission shows a weak dependence with average energy that is not indicated in the previous work by *Germany et. al.* [1994a,b; 1990]. This effect is small (<10% at 10 keV) and is not included in the analysis shown below.

The expected auroral intensities are modeled with a two-stream energy deposition code [*Richards and Torr, 1990*] assuming an incident Gaussian energy distribution. A two-stream model can serve well in cases such as the present which emphasize energy deposition and column intensities. Our two-stream code gives excellent agreement with more detailed multistream models [e.g. *Strickland et al.*, 1983; *Daniell and Strickland*,1986]. Emission cross sections of N_2 LBH are those of *Ajello and Shemansky* [1985] with the downward scaling of 13% of *Ajello et al.*, [1991]. The LBH emissions are modeled based on their relative cross sections as given by *Ajello and Shemansky* [1985] without attempting to construct a highly detailed synthetic spectrum. Similarly, potential atomic nitrogen emissions within the UVI spectral bandpass are not modeled in this preliminary analysis. This will be added in future analyses. The primary effect of neglecting these emissions, principally the 149.3 nm emission, will be to slightly overstate the actual LBH brightness.

Since UVI images include auroral and airglow emissions, the images must have both instrumental and airglow backgrounds removed before analyzing. Airglow is approximated from the image by assuming pixels with similar values of solar zenith angle will have similar airglow emissions, using a technique similar to that discussed by *Lummerzheim et al.*, [1997]. The analysis below is limited to the nightside aurora so potential errors from airglow removal are minimized.

The image data must be registered onto a regular magnetic latitude-MLT grid before image ratios can be calculated. This ensures the pixels used in the image ratios correspond to the same location even though the two images are not temporally coincident. The image coordinates are computed for a magnetic apex coordinate system [*Richmond*, 1995] with MLT being the corresponding local time. The registered images have a spatial resolution of 0.5 degrees in both latitude and longitude. This is only slightly larger than the instrument resolution from apogee. Temporal and spatial changes between the two image exposures used in the ratio may result in edge effects in which the inner and outer edges of the oval region may be anomalously large. These effects have been trapped where possible.

Data

Incident energy characteristics are derived from a single LBHl and two LBHs images taken on May 19, 1996 with the POLAR spacecraft near an apogee distance of 9 Earth radii. The images represent 37 second integrations beginning at 21:43:20, 21:42:06, and 21:44:33 UT, respectively. The images were chosen to be coincident with a DMSP overflight through the nightside auroral oval during the same period. May 19, 1996 is a period in which several ISTP spacecraft are situated in key regions of geospace with GEOTAIL crossing into the Earth's magnetosphere, WIND and INTERBALL upstream of the bow shock, POLAR at apogee, and several overflights of DMSP and NOAA spacecraft. Due to space limitations, comparison will be made only with the DMSP data.

The Defense Meteorological Satellite Program (DMSP) series satellites are polar-orbiting, sun-synchronous satellites with a nominal altitude of 830 km and a period of 101 minutes. DMSP F12 carries the SSJ/4 auroral particle spectrometer capable of measuring electron and ion particle fluxes with energies between 30 eV and 30 keV. The detectors are oriented toward the satellite zenith and produce a complete energy spectrogram once each second. From the measured energy spectra the incident energy flux and average energy (integral energy flux divided by total number flux in the range 460 eV to 30 keV) of the auroral particles can be determined. These parameters are to be compared with UVI estimates of energy flux and average energy.

Images from UVI show auroral brightening beginning near 17:30 UT and continuing throughout the remainder of the day until 2:30 UT on May 20, 1996. A substorm beginning at 20:20 UT on May 19 expanded throughout the nightside leading to a general thickening of the nightside oval. Remnants of that thickening were still present in the selected images. At 21:15 UT an additional intensification began on the poleward boundary. Throughout the period examined here the poleward boundary intensification continued to brighten, an important fact that will be further discussed below. Thus the nightside auroral form is composed of a stable equatorward arc and a dynamic poleward arc. There was no significant dayside auroral emission with the dynamic auroral activity being confined to the night side.

Energy maps are presented in Figure 1 as derived from LBH images. UVI is looking down in the near nadir direction (despun platform offset angle equal to 2.6 degrees). The average energy map (Eavg) is calculated from the ratio of LBHl and LBHs images and has a time resolution set by the time encompassed by the two images. The energy flux map (Eflux) is calculated from the LBHl image alone and therefore has a higher time resolution than the average energy map.

The overflight by the DMSP F12 satellite is shown by the colored ground track which corresponds to the 5 minute period from 21:41 to 21:46 UT. We wish to compare the *in situ* DMSP observations with those derived from analysis of the UVI images. This is done by plotting DMSP energy parameters along its ground track (mapped along the magnetic field line from the spacecraft altitude of roughly 830 km) and then superimposing values derived from UVI images (with an assumed altitude of 120 km) for the same spatial locations. Note that since the two instruments have different time resolutions the comparisons along the ground will be coincident for only a limited time corresponding to the UVI integration time. Furthermore, DMSP samples a much smaller volume in a single observation that does the Ultraviolet Imager. Also, DMSP samples the spatial structure of the aurora in an essentially linear fashion along its ground track while UVI samples the same structure in a two dimensional fashion seeing in a single pixel parts of the aurora that is just off the DMSP ground track. If we assume, however, that the overall auroral morphology is roughly stable over the 5 minute DMSP overflight and homogeneous along the arc orthogonal to the DMSP path we can compare values from the two instruments along the entire overflight.

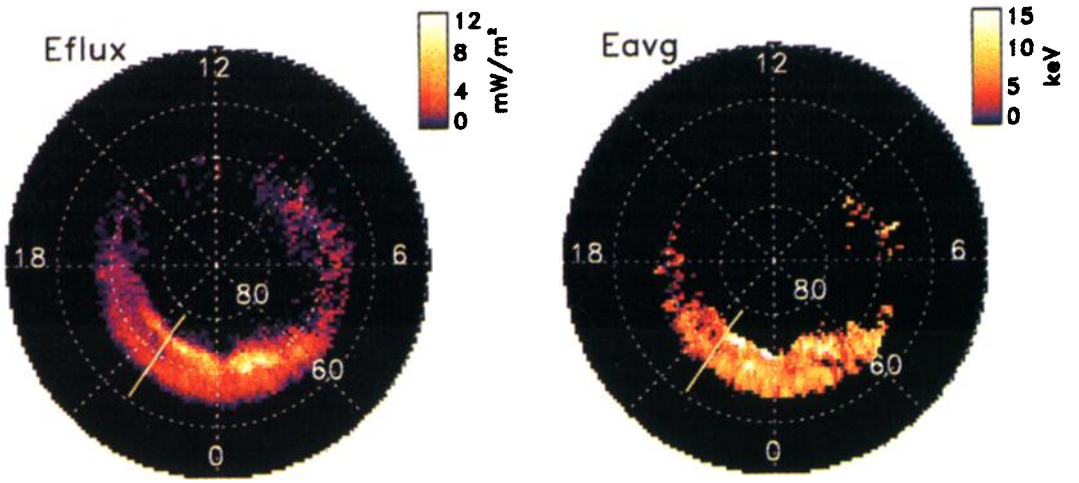

Figure 1. Auroral images and energy maps in MLAT-MLT coordinates where MLAT is an apex magnetic latitude and MLT is the correspond local time. The energy maps correspond to incident energy flux (Eflux) and average energy (Eavg) and are derived from images taken using the long wavelength LBH filter (LBHl, 21:43:20 UT) and the short wavelength filter (LBHs, 21:42:06 UT). The ground track of the DMSP F12 spacecraft is shown for the energy maps.

In situ observations of incident energy flux and average energy from the DMSP auroral spectrometers are shown in Figure 2 as solid curves. The 1 second DMSP data has been averaged to match the UVI 37 second integration period. Crosses represent values from UVI energy maps corresponding to the ground tracks. The vertical lines correspond to the beginning of each UVI image integration. The mean energy profile is a composite of two profiles derived from the two LBHs images. The LBHs image at 21:42:06 UT was used for pixel locations corresponding to DMSP locations before 21:43:30 UT (the equatorward portion of the aurora). The poleward portion was derived from the second LBHs image. The dashed lines represent estimates of the 1 sigma uncertainty levels for each parameter

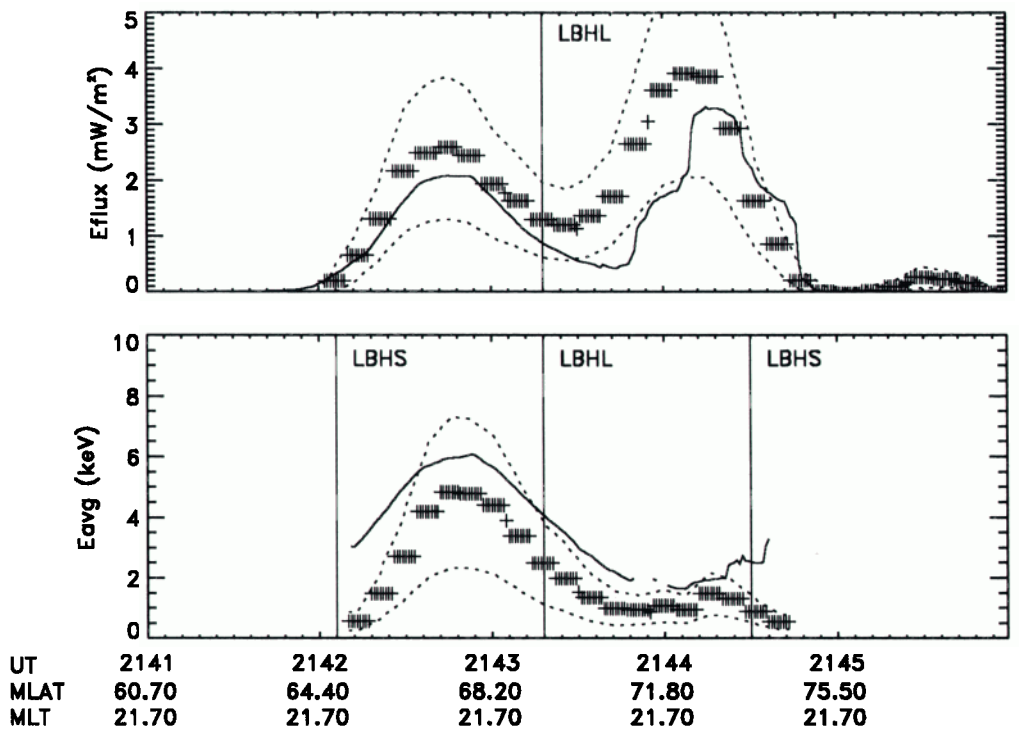

Figure 2. Comparisons of energy flux and average energy along the ground track of the DMSP satellite. Solid lines are DMSP data, crosses are UVI pixel values taken from the energy maps. DMSP average energy values are only shown for incident fluxes greater than 0.1 mW/m^2. The 1 second DMSP data has been averaged to match the UVI 37 second integration period. The vertical lines correspond to the beginning of each UVI image integration. The mean energy profile is a composite of two profiles derived from the two LBHs images (see text). The dashed lines represent the 1 sigma uncertainty levels for each parameter.

and include contributions from the LBH cross sections (22%), the modeling process (25%), the instrumental calibration (25%) and pixel-dependent Poisson signal statistics.

Discussion

Because of the dynamic nature of the auroral event, using only the earlier of the two LBHs images was insufficient to properly characterize the mean energy distribution for comparison with DMSP observations. On the poleward boundary the *in situ* DMSP observations showed consistently higher mean energy than is derived using the first LBHs image (not shown). This is consistent with an increase in brightness on the poleward boundary after the time of the first LBHs image which is what is seen during this event. Recall that the poleward boundary is brightening and expanding throughout this event. In other words, by the time the DSMP satellite reached the northern boundary the incident flux had increased over what was seen in the UVI image taken over a minute previously. Thus the assumption made above that the oval morphology is unchanging during the 5 minute period shown in Figure 2 is not valid for the northern boundary. It does, however, appear to be valid for the remainder of the auroral region. Including the second LBHs image correctly estimates the mean energy for the entire DMSP ground track through the auroral region.

In this paper, UVI images have been used to estimate the magnitude of the incident energy flux over the entire auroral zone. The inferred energy parameters generally agree in magnitude and morphology with selected DMSP overflights. The fluxes inferred from UVI images do not exhibit the same spatial or temporal resolution as the *in situ* measurements but offer a global perspective unattainable from single satellite passes. Figure 1 illustrates the potential of analysis based on Ultraviolet Imager data. The images allow quantitative estimates across extended regions of the auroral zone and are not restricted to a single ground track. Continued comparison with *in situ*, ground based, and other imaging observations is needed to build confidence in this approach. Such studies are currently underway.

Acknowledgments. This work was supported, in part, under U. Washington contract 256730 to the University of Alabama in Hunstville and NASA grant NAG5-3170 to the University of Washington. Work at the University of Alaska was supported by NASA grant NAG5-1097. A. Richmond kindly supplied the database upon which the apex coordinates are based. The authors gratefully acknowledge the many helpful comments of the reviewers.

References

Ajello, J. M., and D. E. Shemansky, A reexamination of important N_2 cross sections by electron impact with application to the dayglow: The Lyman-Birge-Hopfield band system and N I (119.99nm), *J. Geophys. Res.*, *90*, 9845, 1985.

Ajello, J. M., D. E. Shamansky, and G. K. James, Cross sections for production of H(2p, 2s, 1s) by electron collisional dissociation of H_2, *Astrophys. J.*, *371*, 422, 1991.

Daniell, R. E., Jr., and D. J. Strickland, Dependence of auroral middle UV emissions on the incident electron spectrum and neutral atmosphere, *J. Geophys. Res.*, *91*, 321, 1986.

Germany, G. A., M. R. Torr, D. G. Torr, and P. G. Richards, Use of FUV auroral emissions as diagnostic indicators, *J. Geophys. Res.*, *99*, 383, 1994a.

Germany, G. A., D. G. Torr, P. G. Richards, M. R. Torr, and S. John, Determination of ionospheric conductivities from FUV auroral emissions, *J. Geophys. Res.*, *99*, 23297, 1994b.

Germany, G. A., M. R. Torr, P. G. Richards, and D. G. Torr, The dependence of modeled OI 135.6 and N_2 LBH auroral emissions on the neutral atmosphere, *J. Geophys. Res.*, *95*, 7725, 1990.

Lummerzheim, D., M. Brittnacher, D. Evans, G. A. Germany, G. K. Parks, M. H. Rees, and J. F. Spann, High time resolution study of the hemispheric energy flux carried by energetic electrons into the ionosphere during the May 19/20 auroral activity, *Geophys. Rev. Lett.*, in press, 1997.

Lummerzheim, D., M. H. Rees, J. D. Craven, and L. A. Frank, Ionospheric conductances derived from DE-1 auroral images, *J. Atmos. Terr. Phys.*, *53*, 281, 1991.

Richmond, A. D., Ionospheric electrodynamics using magnetic apex coordinates, *J. Geomag. Geoelectr.*, *47*, 191, 1995.

Richards, P. G., and D. G. Torr, Auroral modeling of the 3371 A emission rate: Dependence on characteristic electron energy, *J. Geophys. Res.*, *95*, 10337, 1990.

Strickland, D. J., J. R. Jasperse, and J. A. Whalen, Dependence of auroral FUV emissions on the incident electron spectrum and neutral atmosphere, *J. Geophys. Res.*, *88*, 8051, 1983.

Torr, M. R., D. G. Torr, M. Zukic, R. B. Johnson, J. Ajello, P. Banks, K. Clark, K. Cole, C. Keffer, G. Parks, B. Tsurutani, J. Spann, A far ultraviolet imager for the International Solar-Terrestrial physics mission, *Space Sci. Rev.*, *71*, 329, 1995.

M. Brittnacher, L. Chen, G. Parks, Geophysics Program, Box 351650, University of Washington, Seattle WA 98195.

J. Cumnock, Space Physics Research Laboratory, University of Michigan, 2455 Hayward Rm 2517, Ann Arbor, MI 48109.

G. Germany, Center for Space Plasma and Aeronomic Research, OB 348, University of Alabama in Huntsville, AL 35899 (e-mail: germanyg@cspar.uah.edu).

D. Lummerzheim, Geophysical Institude, Fairbanks, AK 99775.

F. Rich, Geophysics Dir., USAF Phillips Laboratory (PL/GPS), Hanscom AFB, MA 01731.

P. Richards, Computer Science Department, OB 348, University of Alabama in Huntsville, AL 35899.

J. Spann, Space Science Laboratory, NASA Mail Code ES83, NASA Marshall Space Flight Center, Huntsville AL 35812.

(Received September 30, 1996; revised March 19, 1997; accepted March 19, 1997.)